European Radiology (2019) 29:3200–3209
https://doi.org/10.1007/s00330-018-5763-x

COMPUTER APPLICATIONS

Preoperative radiomic signature based on multiparametric magnetic resonance imaging for noninvasive evaluation of biological characteristics in rectal cancer

Xiaochun Meng[1] · Wei Xia[2] · Peiyi Xie[1] · Rui Zhang[2] · Wenru Li[1] · Mengmeng Wang[2] · Fei Xiong[1] · Yangchuan Liu[2] · Xinjuan Fan[3] · Yao Xie[1] · Xiangbo Wan[4] · Kangshun Zhu[5] · Hong Shan[6] · Lei Wang[7] · Xin Gao[2]

Received: 18 May 2018 / Revised: 21 August 2018 / Accepted: 14 September 2018 / Published online: 9 November 2018

Abstract

Objectives To develop and validate radiomic models in evaluating biological characteristics of rectal cancer based on multiparametric magnetic resonance imaging (MP-MRI).

Methods This study consisted of 345 patients with rectal cancer who underwent MP-MRI. We focused on evaluating five postoperative confirmed characteristics: lymph node (LN) metastasis, tumor differentiation, fraction of *Ki-67*-positive tumor cells, human epidermal growth factor receptor 2 (*HER-2*), and *KRAS-2* gene mutation status. Data from 197 patients were used to develop the biological characteristics evaluation models. Radiomic features were extracted from MP-MRI and then refined for reproducibility and redundancy. The refined features were investigated for usefulness in building radiomic signatures by using two feature-ranking methods (MRMR and WLCX) and three classifiers (RF, SVM, and LASSO). Multivariable logistic regression was used to build an integrated evaluation model combining radiomic signatures and clinical characteristics. The performance was evaluated using an independent validation dataset comprising 148 patients.

Results The MRMR and LASSO regression produced the best-performing radiomic signatures for evaluating *HER-2*, LN metastasis, tumor differentiation, and *KRAS-2* gene status, with AUC values of 0.696 (95% CI, 0.610–0.782), 0.677 (95% CI, 0.591–0.763), 0.720 (95% CI, 0.621–0.819), and 0.651 (95% CI, 0.539–0.763), respectively. The best-performing signatures for evaluating Ki-67 produced an AUC value of 0.699 (95% CI, 0.611–0.786), and it was developed by WLCX and RF algorithm. The integrated evaluation model incorporating radiomic signature and MRI-reported LN status had improved AUC of 0.697 (95% CI, 0.612–0.781).

Conclusion Radiomic signatures based on MP-MRI have potential to noninvasively evaluate the biological characteristics of rectal cancer.

Key Points

- *Radiomic features were extracted from MP-MRI images of the rectal tumor.*
- *The proposed radiomic signatures demonstrated discrimination ability in identifying the histopathological, immunohistochemical, and genetic characteristics of rectal cancer.*
- *All MRI sequences were important and could provide complementary information in radiomic analysis.*

Keywords Rectal neoplasms · Magnetic resonance imaging · Algorithms

Xiaochun Meng and Wei Xia are primary authors and contributed equally to this work.

Electronic supplementary material The online version of this article (https://doi.org/10.1007/s00330-018-5763-x) contains supplementary material, which is available to authorized users.

✉ Lei Wang
wangl9@mail.sysu.edu.cn

✉ Xin Gao
xingaosam@yahoo.com

Extended author information available on the last page of the article

Abbreviations

AUC	Area under the receiver operating characteristic curve
CRC	Colorectal cancer
DCE	Dynamic contrast-enhanced
DWI	Diffusion-weighted imaging
HER-2	Human epidermal growth factor receptor 2
LASSO	Least absolute shrinkage and selection operator
MP-MRI	Multiparametric magnetic resonance imaging
MRMR	Minimum redundancy maximum relevance

RF Random forest
WLCX Wilcoxon rank-sum test

Introduction

Colorectal cancer (CRC) is the third most commonly diagnosed cancer in the USA [1]. The most serious issue is that from 2000 to 2013, CRC incidence rates increased 22% in US adults younger than 50 years of age. Rectal cancer accounts for about 28% of CRC cases in the USA [2].

Different biological characteristics of CRC may lead to different treatment responses and prognoses. For example, anti-epidermal growth factor receptor (anti-EGFR) therapy has been proven to be of no benefit to patients with a *RAS* mutation [3–5]. Overexpression of human epidermal growth factor receptor 2 (*HER-2*) may be associated with metastasis and could be used as a negative predictive biomarker for anti-EGFR therapy [6]. Expression of *Ki-67* contributes to enhancement of the proliferation of malignant tumors, and the *Ki-67* index has been considered as a biomarker of tumor aggressiveness [7]. Higher nodal stage always presents a higher risk of recurrence, and oxaliplatin appears to have increased benefit for patients with these statuses [8]. Patients with well-differentiated tumors have been found to have better overall survival rates [9]. Thus, identifying the biological characteristics of CRC may contribute to a tailored treatment and may increase survival rates.

Undoubtedly, histopathology and molecular sequencing are the main methods of determining biological characteristics. However, the spatial and temporal heterogeneities that tumors show vary from gene to tissue [10]. The risks of invasive sampling and potential complications [11] limit the application of these methods in real-time monitoring of disease progression and tumor biological characteristics. However, medical imaging can capture tumor macroscopic imaging features that reflect microscopic changes in genomic and proteomic patterns [12], and it offers the ability to comprehensively, noninvasively, and repeatedly evaluate tumor biological characteristics and monitor tumor response to treatment in real time. In particular, multiparametric magnetic resonance imaging (MP-MRI) can reveal the phenotypic differences of tumors to a certain extent by showing signal intensity and enhancement characteristics [13]. Besides, in comparison with a mono-modality imaging method such as computed tomography (CT), MP-MRI can provide more valuable data for radiomics through high-throughput extraction of quantitative image features [14].

With radiomic techniques, the quantitative imaging features could be extracted and used for subsequent machine learning-based analysis to generate imaging biomarkers for evidence-based clinical decision-making [15]. Recent studies of CRC have showed encouraging evidence that radiomic features can be applied to predict characteristics including lymph node metastasis [16], outcomes of neoadjuvant chemoradiation [17–19], and tumor development stage [20]. However, there have been no reports of radiomic studies using MP-MRI with larger data and independent testing. More importantly, the studies that have been done mainly focused on the evaluation of one characteristic, but the oncogenesis, metastasis, and cancer reaction to treatment are affected by multiple tumor biological characteristics, and thus, a comprehensive radiomic analysis investigating the evaluation of multiple biological characteristics is required. Besides, in the current radiomics workflow [15], it is important to figure out the optimal combination of feature selection and classifier modeling methods to achieve the best performance.

Therefore, in this study, we tried to establish and validate radiomic signatures based on MP-MRI to noninvasively evaluate biological characteristics of rectal cancer.

Materials and methods

Patients profiles, image acquisition, and biological tests

Retrospective data evaluation was approved by the local ethics committee. The requirement for evidence of informed consent was waived because of the retrospective nature of our study. Medical data for all patients who underwent radical resection for rectal cancer at the Sixth Affiliated Hospital of Sun Yat-sen University (Guangzhou, China) between June 2013 and October 2016 were collected retrospectively. After we excluded the patients who received preoperative therapy, we enrolled a total of 345 patients who underwent rectal MRI within 2 weeks before surgery and for whom there was postoperative data on *HER-2*, *Ki-67*, lymph node metastasis status, tumor differentiation, and/or *KRAS* gene mutation.

For each biological characteristic, the patients for whom there were data available about the characteristic were classified as a subgroup, for a total of five subgroups. In each subgroup, the patients were divided into two labeled classes by dichotomizing the characteristic on the basis of its clinical usefulness and its distribution, and the *Ki-67* dividing threshold of 40%, which is supported by previous studies [21]. The principles of divisions are shown in Table 1.

Of those 345 patients, 197 treated between June 2013 and December 2015 were assigned to the discovery dataset, and 148 patients treated between January 2016 and October 2016 were assigned to an independent validation dataset. Patients' clinical characteristics, including age, sex, carcinoembryonic antigen (CEA) level, and preoperative/postoperative clinical stage were obtained from medical records. The details of rectal MRI protocol, patient's profiles, and biological test results are presented in supplements A and B of this article.

Table 1 The principles of labeling patients in each subgroup

Label	*HER-2*	*Ki-67*	Differentiation	Lymph node metastasis	*KRAS-2*
1	> 0	≥ 40%	Well-differentiated	Metastasis	Mutation
0	= 0	< 40%	Others	No metastasis	Wild-type

Radiomic feature extraction

For each patient, the tumor volume of interest (VOI) was determined by manual delineating tumor contours slice-by-slice on T2W-MRI images using Medical Imaging Interaction Toolkit (MITK) software (version 2013.12.0; http://www.mitk.org/). All MP-MRI volumes were resampled to the same resolution. The T1W, DWI, and DCE-MRI volumes were aligned to T2W-MRI using in-house software [22] based on open-source Insight Segmentation and Registration Toolkit (ITK, version 4.7.2; https://itk.org/). As a result, the VOI generated from T2W-MRI could be used in all MRI sequences.

The feature-extraction algorithm was developed and modified on the basis of an open access program [23, 24] (https://github.com/mvallieres/radiomics/) and executed with MATLAB (version 2015a; MathWorks). Radiomic features were extracted from MRI sequences for each patient. The radiomic features that can be divided into five categories [17, 23, 25]: 9 geometric features, 14 first-order statistical features, 56 texture features, 560 wavelet features, and 5 time-intensity curve (TIC) features. Prior to the computation of texture features, all volumes were resampled to an isotropic voxel size of axial plane resolution using cubic interpolation and the full intensity range of the tumor region was quantized to 32 gray levels. The detailed radiomic features list was described in supplement C.

Feature selection and classifier modeling

The manual delineation may introduce a degree of uncertainty in determination of tumor VOI. And some of the features extracted from the manual delineated tumor VOI may have low reproducibility when the tumor VOI was manually delineated by different persons or at different times. To eliminate the features with low reproducibility [16], two radiologists (radiologist 1 with 6 years of experience in MRI interpretation and radiologist 2 with 5 years of experience) were assigned to delineate the tumor VOI. Radiologist 1 carried out a sequence of delineations at two different times and radiologist 2 carried out a once-only delineation. The features obtained were computed after each delineation was carried out. The interclass and intraclass correlation coefficients (ICCs) of the interobservers (radiologist 1 vs radiologist 2) and the intraobserver (radiologist 1) were computed. A large value of the ICC represents a high degree of reproducibility and vice versa. As a result, features of low interclass or intraclass ICC values were considered to be of low reproducibility and were therefore removed.

To identify redundant features, the pair-wise feature correlations were calculated to build Pearson's correlation matrixes [15]. If two features are highly correlated, the mean absolute correlation of each feature was calculated and the feature with the largest mean absolute correlation was considered to be redundant and eliminated.

After elimination of redundant features and the features with low reproducibility, we used feature-ranking algorithms [26] to identify the most important features on the basis of a heuristic scoring criterion, and only the top-ranked features were kept. We used a univariate ranking method (Wilcoxon rank-sum test [WLCX]) and a multivariate ranking method (minimum redundancy maximum relevance [MRMR]) [26–28]. WLCX is a representative univariate method and achieved best performance in a study investigating 14 feature selection methods [26]. MRMR is a representative and highly cited multivariate method [27] and had the best performance among 13 feature selection methods [28].

The top-ranking radiomic features were input to a classifier to build a radiomic signature for the evaluation of each biological characteristic. Three classifiers were evaluated in this study, including the least absolute shrinkage and selection operator (LASSO) [16], the random forest (RF) algorithm [26, 29], and the support vector machine (SVM) [26, 29]. RF achieved the best performance among 179 classifiers based on the 121 different datasets in a large comparative study [29], and SVM achieved the second-best performance and there was no statistically significant difference with RF results. Besides, LASSO was the main method in current radiomic studies [12] and showed excellent performance [16]. Classifiers were trained using 10-fold cross-validation on the discovery dataset to determine the optimal parameter configuration for classifiers. Although some classifiers such as RF and LASSO already have an inherent feature selection/weighting mechanism built into the training, previous studies have shown that adding prior feature ranking procedure may be helpful to improve the final performance [26, 28]. We also performed the training without prior feature ranking to validate the influence of this procedure.

The radiomic signatures were tested on the independent validation dataset, and their discrimination performance were assessed using receiver operating characteristic (ROC) curve analysis and quantified by the area under the ROC curve (AUC) [30]. The radiomic signature with the highest AUC was selected as the optimal radiomic signature.

In addition, we use multivariable logistic regression to build integrated evaluation models with the discovery dataset

by using the optimal radiomic signature and clinical characteristics (age, sex, CEA level) as input. To build an integrated evaluation model, we determined the optimal combinations of the optimal radiomic signature and all subsets of clinical characteristics by using the Akaike information criterion [16]. The discrimination ability of the integrated evaluation model was also tested on the independent validation dataset and assessed by the AUC. The DeLong test [31, 32] was used to compare the AUCs for the integrated evaluation model against the corresponding optimal radiomic signature. For lymph node status evaluation, the MRI-reported lymph node status in the preoperative image manual identification report was also compared with radiomic signature. And the integrated evaluation model incorporating MRI-reported lymph node status was tested.

The R software (3.3.2) was used to conduct feature selection, classifier modeling, and statistical analysis. The theory of the feature-ranking algorithms and the introduction and parameter-tuning process of classifiers are described in supplements D and E.

Results

Patient profiles

The patient profiles for subgroups gathered according to biological characteristics are given in Table 2. Label status has already been described in Table 1. As a result of missing data, subgroups have unequal sizes.

Feature selection and acquisition of radiomic signatures

A total of 2534 radiomic features were extracted for each patient. The features with low reproducibility that had intra- or inter-observer ICC of < 0.75 were excluded, so the number of features was reduced to 1547. Subsequently, the pair-wise Pearson correlation coefficients were calculated. The threshold for identifying highly correlated feature pairs was 0.9, leaving 446 features for *Ki-67*, 445 for *HER-2*, 456 for lymph node metastasis, 449 for differentiation, and 427 for *KRAS-2,* respectively. The remaining features were ranked by WLCX and MRMR, and then, the top 50 features were selected.

The classifiers RF, LASSO, and SVM were trained on the discovery dataset using the top-ranked features, which ranged from 5 to 50 with increments of 5, to build radiomic signatures. The discrimination abilities of radiomic signatures were tested on the independent validation dataset (Table S2). For each subgroup, the optimal signature with the highest AUC was selected. The optimal signature for evaluating *Ki-67* status was obtained by combining the top 20 features selected by WLCX and classifier RF. The combination of the top 10 features selected by MRMR and classifier LASSO provided the optimal radiomic signatures in evaluating *HER-2*, lymph node metastasis, tumor differentiation, and *KRAS-2* gene status. The features used in building optimal radiomic signatures along with their formulas are given in Table S3.

Table 3 shows how each optimal signature performed. The AUCs of optimal signatures were also compared with a random guess by chance with an AUC of 0.5; the *p* values from the DeLong test are given in Table 3. Figure 1 shows the ROC curves for each biological characteristic; the point on the discovery ROC curve that was closest to the upper left corner was selected as the cutoff [33]. The radiomic signatures allowed scoring of each patient, and the cutoff was used as the score threshold. Patients' scores below or above the cutoff were considered to be labeled 0 or 1. Then, the corresponding accuracy, sensitivity, and specificity values were calculated (Table 3). Figure 2 shows examples of MRI images used. In the clinical setting where the extracted radiomic features were used as input, the radiomic signatures scored each patient. For *HER-2*, the cutoff for a radiomic signature was 0.681, one patient's score of 1.556 was higher than the score of 0.681 identified to have a label of 1 (*HER-2* > 0), and another patient's score was identified to have a label of 0 (*HER-2* = 0).

There was a significant difference in *HER-2* label between discovery and validation set (Table 2). To evaluate the impact of this difference, we resampled the validation data and calculated the AUC of validation 1000 times. In each resampling, 36 negative samples were randomly selected to make sure the ratio of positive to negative samples in the resampled validation set was equal to the ratio in discovery set. The AUC of resampled validation sets was 0.695 ± 0.031 (mean value ± standard deviation), and it was very close to the AUC of whole validation set (0.696). This demonstrated that the proposed radiomic signature was insensitive to the distribution of samples and had good stability.

For lymph node status evaluation, we calculated the accuracy of MRI-reported lymph node status from the preoperative image report. The MRI-reported lymph node status has accuracy, sensitivity, and specificity of 0.613, 0.704, and 0.559, respectively. The radiomic signature has similar performance with the MRI-reported lymph node status.

Radiomic heat maps for all patients are shown in Figure S1. These represent the values of imaging features used in the optimal signatures for all patients, the scores of the radiomic signatures, and the corresponding labels for each patient.

Performance of integrated evaluation models

The integrated evaluation models which combined the optimal radiomic signature and clinical characteristics (age, sex, and CEA level) showed no statistically significant ($p > .05$) improvements in AUCs in comparison with radiomic signatures. For lymph node status evaluation, after the addition of MRI-reported lymph node status, AUC of the integrated evaluation model was significantly ($p < .05$) improved from 0.752

Table 2 Patient profiles of each subgroup

Characteristic	Age (years)	Sex (%)		Label (%)		Total
		M	*F*	0	1	
HER-2						
Discovery	58.99 ± 11.83	110 (60.1)	73 (39.9)	61 (33.3)	122 (66.7)	183
Validation	60.85 ± 12.30	87 (62.1)	53 (37.9)	68 (48.6)	72 (51.4)	140
p value	.186	.691		.011		
Ki-67						
Discovery	59.37 ± 11.71	111 (59.7)	75 (40.3)	74 (39.8)	112 (60.2)	186
Validation	61.06 ± 12.51	87 (61.7)	54 (38.3)	51 (36.2)	90 (63.8)	141
p value	.265	.706		.524		
Lymph node metastasis						
Discovery	59.48 ± 11.77	114 (60.0)	76 (40.0)	128 (67.4)	62 (32.6)	190
Validation	61.10 ± 12.44	92 (63.0)	54 (37.0)	83 (56.8)	63 (43.2)	146
p value	.209	.608		.089		
Differentiation						
Discovery	59.16 ± 11.78	108 (61.0)	69 (39.0)	124 (70.1)	53 (29.9)	177
Validation	61.28 ± 12.37	84 (61.3)	53 (38.7)	108 (78.8)	29 (21.2)	137
p value	.141	1.000		.127		
KRAS-2						
Discovery	59.76 ± 11.96	98 (58.7)	69 (41.3)	103 (61.7)	64 (38.3)	167
Validation	60.02 ± 12.27	62 (62.6)	37 (37.4)	56 (56.6)	43 (43.4)	99
p value	.879	.667		.550		

Ages are shown as mean ± standard deviation; other data are number of patients, with percentage in parentheses. The *p* values are derived from the comparison between the discovery set and the validation set, using the chi-square test for sex and label or the Wilcoxon rank-sum test for age

to 0.804 in the discovery dataset, and improved from 0.677 to 0.697 in the validation dataset ($p = 0.470$). The formula and performance of the integrated evaluation models for lymph node metastasis are listed in Table 4.

Table 3 Performance of optimal radiomic signatures

Characteristic	AUC	95% CI	*p* value	Cutoff	ACC	SEN	SPE
HER-2							
Discovery	0.707	0.627,0.787	.000	0.681	0.678	0.713	0.607
Validation	0.696	0.610,0.782	.000	–	0.621	0.667	0.574
Ki-67							
Discovery	0.607	0.525,0.689	.014	0.398	0.570	0.622	0.536
Validation	0.699	0.611,0.786	.000	–	0.582	0.863	0.422
Lymph node metastasis							
Discovery	0.752	0.682,0.822	.000	−0.774	0.668	0.774	0.617
Validation	0.677	0.591,0.763	.000	–	0.610	0.762	0.494
Differentiation							
Discovery	0.675	0.591,0.759	.000	−0.855	0.622	0.679	0.597
Validation	0.720	0.621,0.819	.000	–	0.606	0.759	0.565
KRAS-2							
Discovery	0.669	0.586,0.753	.000	−0.307	0.665	0.531	0.748
Validation	0.651	0.539,0.763	.009	–	0.616	0.581	0.643

p values were derived from the DeLong test of comparing AUCs between radiomic signatures and random guess by chance, with an AUC of 0.5

The cutoffs were the same for the discovery and the validation set. *AUC* area under the curve, *ACC* accuracy, *CI* confidence interval, *SEN* sensitivity, *SPE* specificity

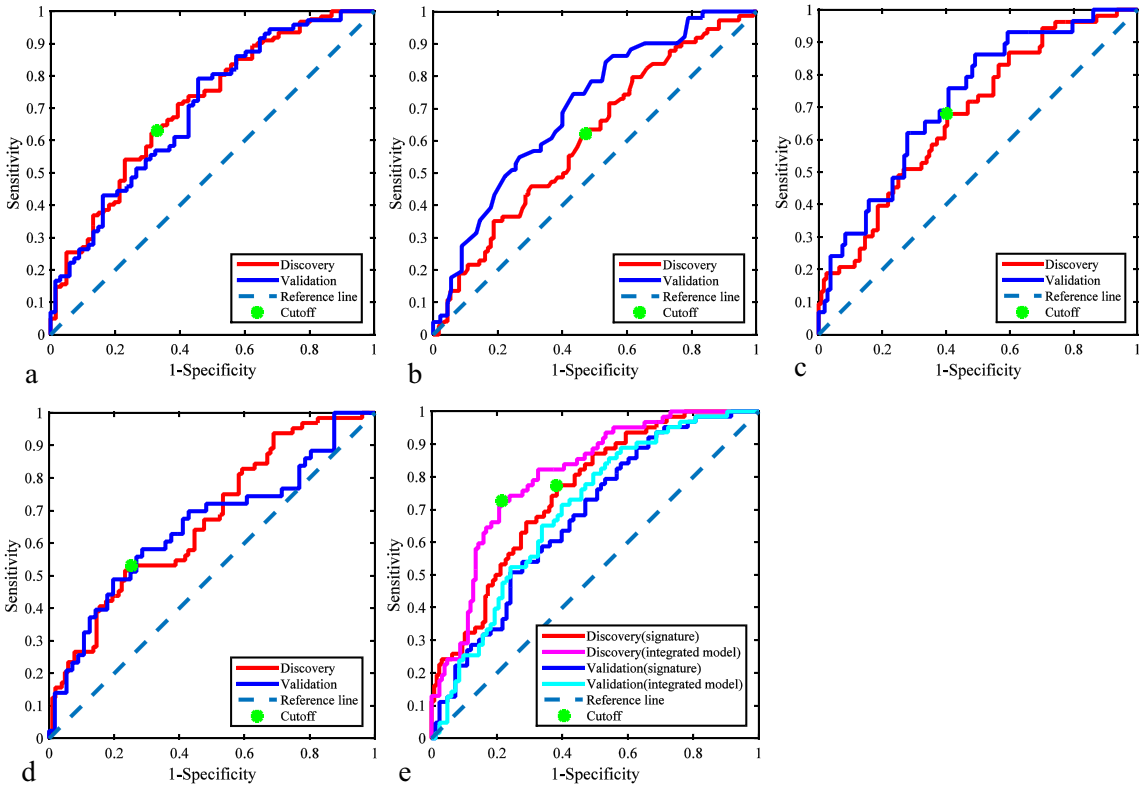

Fig. 1 The receiver operating characteristic curves of radiomic signatures. **a** *HER-2*. **b** *Ki-67*. **c** Tumor differentiation. **d** *KRAS-2*. **e** Lymph node metastasis. For lymph node metastasis, the ROC curves of integrated evaluation model were also plotted

Discussion

We tried to find any association between MRI features and biological characteristics by using radiomic approaches. Our main findings concern radiomic signatures and integrated evaluation models in the evaluation of five biological characteristics: level of *HER-2*, fraction of *Ki-67*-positive tumor cells, lymph node metastasis, tumor differentiation, and *KRAS* gene mutation in exon 2 codons 12 and 13 (*KRAS-2*).

For each MP-MRI modality, we extracted most of the features mentioned in the current literatures. After evaluating features and eliminating redundancies, we used the remaining features to build radiomic signatures, and we investigated two feature-ranking methods (WLCX, MRMR) and three classifiers (LASSO, RF, and SVM). Other researchers have reported excellent performance for these ranking methods and classifiers [16, 26, 29, 34]. Moreover, the tools were publicly available, which ensures their reproducibility. For all biological characteristics, the optimal radiomic signatures showed statistically significant discrimination ability. For lymph node evaluation, radiomic signature had similar performance with MRI-reported lymph node status. The integrated evaluation model incorporating radiomic signature and MRI-reported lymph node status showed significant improvements. The results indicate that the machine learning-derived knowledge and manual identification knowledge are mutually complementary.

In the five optimal radiomic signatures, four of the signatures were built using the top 10 features selected by MRMR, and one was built using the top 20 features from WLCX. Even though RF and LASSO have built-in feature selection mechanism, it showed that the prior feature ranking before training could improve the final performance of classifiers. MRMR ranked features according to multivariate interaction within the features; it was one of the most powerful feature-selection methods and showed good performance in several studies [28, 34, 35]. In contrast, WLCX was a simple univariate feature-ranking method, and it just took the difference of features between two classes into consideration, but it also performed well in some studies [26].

For the features used in optimal radiomic signatures, wavelet features were the majority (15/20 for *Ki-67*, 7/10 for *HER-2*, 8/10 for lymph node metastasis, 7/10 for tumor differentiation, and 7/10 for *KRAS-2*). The wavelet features can quantify intratumor heterogeneity at different scales that cannot be recognized by the naked eye. Several studies also showed that wavelet features had strong prognostic abilities and were important components in building radiomic signatures [25, 35, 36].

There were four MRI sequences used in the feature extraction. After the features were selected and the redundant,

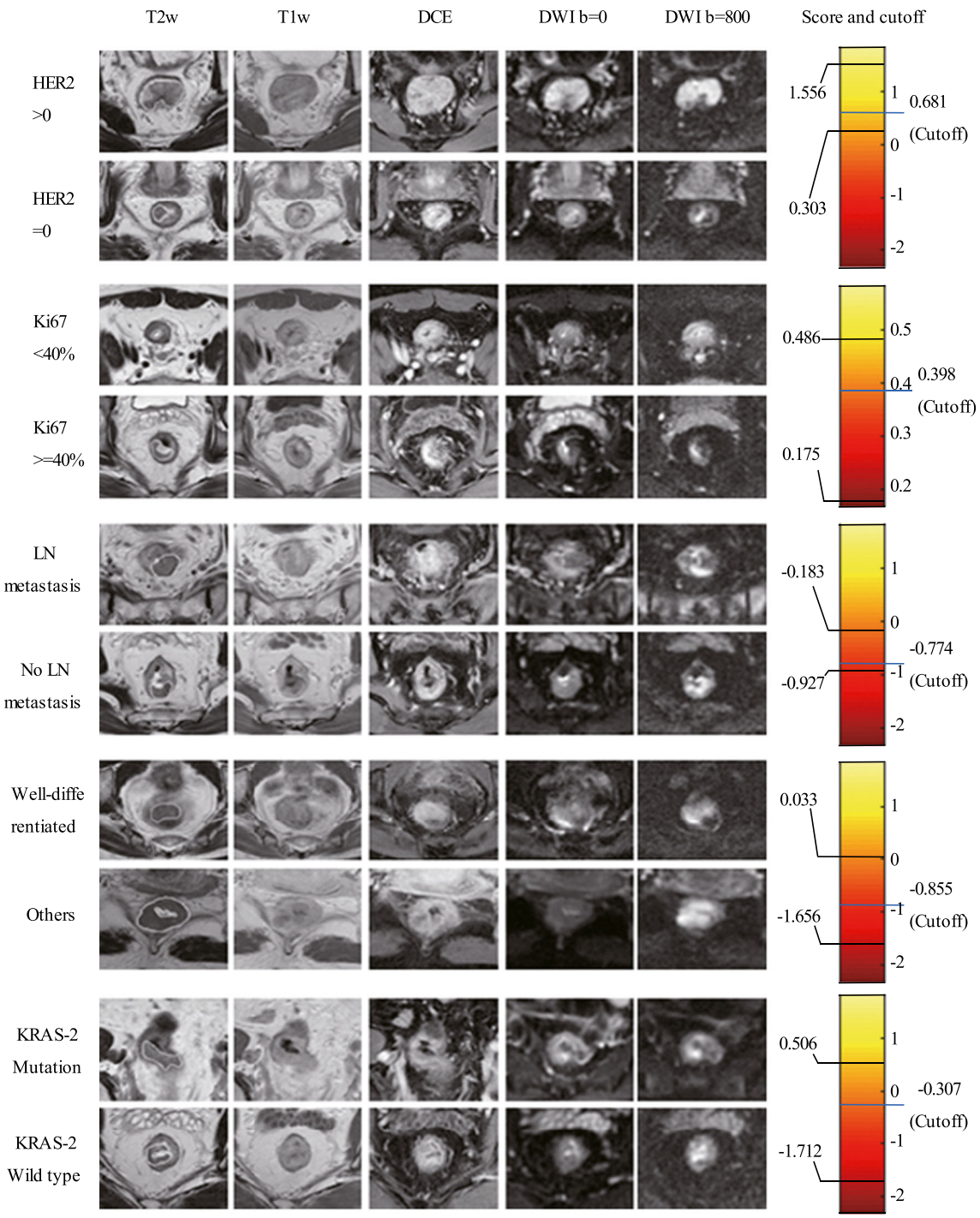

Fig. 2 Preoperative images obtained by multiparametric magnetic resonance imaging and radiomic signature scores of patients with rectal cancer with different biological characteristics. The far-right column lists the corresponding scores of optimal radiomic signatures and the cutoffs

unstable, or inessential features were eliminated, we still were able to find the image features derived from each MRI sequence in the final features used for optimal radiomic signatures, which suggests that all MRI sequences are important and could provide complementary information in radiomic analysis. In particular, ADC maps, DCE-MRI, and T2W-MRI identified the highest number of features in the optimal radiomic signatures of *Ki-67* (7/20), *HER-2* (5/10), and lymph node metastasis (4/10). For the optimal signatures of tumor differentiation, T2W-MRI, and ADC maps revealed the same highest number of features (3/10); for *KRAS-2*, T1W-MRI, and DCE-MRI provided the same highest number of features (3/10).

Choosing a proper classifier was also crucial for obtaining evaluation models with good performance. The LASSO

Table 4 Formulas and performance of the integrated evaluation model

Lymph node metastasis	Formulas	AUC	95% CI	*p*	Cutoff	ACC	SEN	SPE
Discovery	1.021 × signature + 1.286 × report − 0.823 × gender − 0.242	0.804	0.741,0.868	0.024	− 0.518	0.766	0.726	0.786
Validation	–	0.697	0.612,0.781	0.470	–	0.637	0.730	0.566

p value was from the method of Delong in the test of two AUCs between the integrated evaluation model and the corresponding optimal radiomic signature *signature*, optimal radiomic signature, *report* MRI-reported lymph node status, *95% CI* 95% confidence interval of AUC, *ACC* accuracy, *SEN* sensitivity, *SPE* specificity

classifier performed best in evaluating *HER-2*, lymph node metastasis, tumor differentiation, and *KRAS* mutation. It should be noted that LASSO has shown high performance in recent radiomic studies [16, 20, 32, 37]. RF and SVM have been shown to be excellent and popular classifiers in both biomedical and other applications [26, 28, 29], but only RF performed best for evaluating *Ki-67*, and SVM failed to obtain better performance than LASSO or RF. These results indicate that LASSO has certain advantages in radiomic analysis.

Only a few researchers have conducted radiomic analysis that is based on MP-MRI to evaluate tumor characteristics. Recently, Nie et al [17] investigated MP-MRI radiomics analysis of outcomes of neoadjuvant chemoradiation in rectal cancer. Because the study involved only 48 patients, the number of extracted features was limited, and thus, many image features were not taken into account. Furthermore, there was no external independent test for comparison.

One of the limitations of our study is the lack of multi-institutional validation of radiomic signatures. Huang and colleagues [16] reported on the performance of radiomic nomograms for evaluation of lymph node metastasis in CRC based on CT images. Their proposed nomogram performed comparable (CI/AUC = 0.736 and 0.778 for discovery and validation) with our integrated evaluation model did (AUC = 0.804 and 0.697 for discovery and validation), but their patient cohorts differed from ours, and MRI undoubtedly has greater advantages in reflecting tumor heterogeneity, primary tumor T stage, and peripheral soft-tissue invasion for rectal cancer diagnosis. Therefore, much work should to be done in the future to compare the performance of radiomic signatures based on CT and MRI for all biological characteristics in the same patient cohort. Besides tissue characteristics, MRI signal intensity is related to many factors, such as strength and uniformity of the main magnetic field, the sequence used, and the imaging parameters used (TR, TE, trigger angle, and others). Thus, the application of MRI for radiomics has been thought to be complicated by many issues because of the intrinsic difficulty of normalization and regularization of MRI signals [38]. Obviously, much work is necessary to make it practical to use MRI radiomic models clinically, especially for data from different MRI scanners and even from different hospitals.

In conclusion, radiomic signatures have the potential to be used noninvasively in the evaluation of biological characteristics of rectal cancer, which may help in individualizing treatment.

Acknowledgements Medical editor Katharine O'Moore-Klopf, ELS (East Setauket, NY, USA) provided professional English-language editing of this article.

Funding This study has received funding by the National Natural Science Foundation of China [grant number 81571772, 81430041]; Science, Technology Plan Projects of Jiangsu—Society Development Project [grant number BE2017671]; and Foundation for Pearl River Science & Technology Young Scholars of Guangzhou [grant 201610010059].

Compliance with ethical standards

Guarantor The scientific guarantor of this publication is Xin Gao.

Conflict of interest The authors of this manuscript declare no relationships with any companies, whose products or services may be related to the subject matter of the article.

Statistics and biometry No complex statistical methods were necessary for this paper.

Informed consent Written informed consent was waived by the Institutional Review Board.

Ethical approval Institutional Review Board approval was obtained.

Methodology
- retrospective
- diagnostic experimental
- performed at one institution

References

1. Siegel RL, Miller KD, Jemal A (2017) Cancer statistics, 2017. CA Cancer J Clin 67:7–30
2. Siegel RL, Miller KD, Fedewa SA et al (2017) Colorectal cancer statistics, 2017. CA Cancer J Clin 67:177–193
3. Van Cutsem E, Kohne CH, Hitre E et al (2009) Cetuximab and chemotherapy as initial treatment for metastatic colorectal cancer. N Engl J Med 360:1408–1417
4. Heinemann V, von Weikersthal LF, Decker T et al (2014) FOLFIRI plus cetuximab versus FOLFIRI plus bevacizumab as first-line treatment for patients with metastatic colorectal cancer (FIRE-3): a randomised, open-label, phase 3 trial. Lancet Oncol 15:1065–1075
5. Van Cutsem E, Kohne CH, Lang I et al (2011) Cetuximab plus irinotecan, fluorouracil, and Leucovorin as first-line treatment for metastatic colorectal cancer: updated analysis of overall survival

according to tumor KRAS and BRAF mutation status. J Clin Oncol 29:2011–2019
6. Martin V, Landi L, Molinari F et al (2013) HER2 gene copy number status may influence clinical efficacy to anti-EGFR monoclonal antibodies in metastatic colorectal cancer patients. Br J Cancer 108:668–675
7. Brown DC, Gatter KC (2002) Ki67 protein: the immaculate deception? Histopathology 40:2–11
8. Shah MA, Renfro LA, Allegra CJ et al (2016) Impact of patient factors on recurrence risk and time dependency of oxaliplatin benefit in patients with colon cancer: analysis from modern-era adjuvant studies in the Adjuvant Colon Cancer End Points (ACCENT) Database. J Clin Oncol 34:843-+
9. Xiao H, Yoon YS, Hong SM et al (2013) Poorly differentiated colorectal cancers correlation of microsatellite instability with clinicopathologic features and survival. Am J Clin Pathol 140:341–347
10. Burrell RA, McGranahan N, Bartek J, Swanton C (2013) The causes and consequences of genetic heterogeneity in cancer evolution. Nature 501:338–345
11. Robertson EG, Baxter G (2011) Tumour seeding following percutaneous needle biopsy: the real story! Clin Radiol 66:1007–1014
12. Lambin P, Rios-Velazquez E, Leijenaar R et al (2012) Radiomics: extracting more information from medical images using advanced feature analysis. Eur J Cancer 48:441–446
13. Jhaveri KS, Hosseini-Nik H (2015) MRI of rectal cancer: an overview and update on recent advances. AJR Am J Roentgenol 205:W42–W55
14. Dinapoli N, Casa C, Barbaro B et al (2016) Radiomics for rectal cancer. Translational Cancer Research 5:424–431
15. Gillies RJ, Kinahan PE, Hricak H (2016) Radiomics: images are more than pictures, they are data. Radiology 278:563–577
16. Huang YQ, Liang CH, He L et al (2016) Development and validation of a radiomics nomogram for preoperative prediction of lymph node metastasis in colorectal cancer. J Clin Oncol 34:2157−+
17. Nie K, Shi LM, Chen Q et al (2016) Rectal cancer: assessment of neoadjuvant chemoradiation outcome based on radiomics of multiparametric MRI. Clin Cancer Res 22:5256–5264
18. Liu ZY, Zhang XY, Shi YJ et al (2017) Radiomics analysis for evaluation of pathological complete response to neoadjuvant chemoradiotherapy in locally advanced rectal cancer. Clin Cancer Res 23:7253–7262
19. Yankai M, Yuchen Z, Di D et al (2018) Novel radiomic signature as a prognostic biomarker for locally advanced rectal cancer. J Magn Reson Imaging. https://doi.org/10.1002/jmri.25968
20. Liang CS, Huang YQ, He L et al (2016) The development and validation of a CT-based radiomics signature for the preoperative discrimination of stage I-II and stage III-IV colorectal cancer. Oncotarget 7:31401–31412
21. Fluge O, Gravdal K, Carlsen E et al (2009) Expression of EZH2 and Ki-67 in colorectal cancer and associations with treatment response and prognosis. Br J Cancer 101:1282–1289
22. Xia W, Gao X (2014) A fast deformable registration method for 4D lung CT in hybrid framework. Int J Comput Assist Radiol Surg 9:523–533
23. Vallieres M, Freeman CR, Skamene SR, El Naqa I (2015) A radiomics model from joint FDG-PET and MRI texture features for the prediction of lung metastases in soft-tissue sarcomas of the extremities. Phys Med Biol 60:5471–5496
24. Xia W, Chen Y, Zhang R et al (2018) Radiogenomics of hepatocellular carcinoma: multiregion analysis-based identification of prognostic imaging biomarkers by integrating gene data-a preliminary study. Phys Med Biol. https://doi.org/10.1088/1361-6560/aaa609
25. Aerts HJWL, Velazquez ER, Leijenaar RTH et al (2014) Decoding tumour phenotype by noninvasive imaging using a quantitative radiomics approach. Nat Commun. https://doi.org/10.1038/ncomms5006
26. Parmar C, Grossmann P, Bussink J, Lambin P, Aerts HJWL (2015) Machine learning methods for quantitative radiomic biomarkers. Sci Rep. https://doi.org/10.1038/srep13087
27. Peng HC, Long FH, Ding C (2005) Feature selection based on mutual information: criteria of max-dependency, max-relevance, and min-redundancy. IEEE Trans Pattern Anal Mach Intell 27:1226–1238
28. Parmar C, Grossmann P, Rietveld D, Rietbergen MM, Lambin P, Aerts HJWL (2015) Radiomic machine-learning classifiers for prognostic biomarkers of head and neck cancer. Front Oncol. https://doi.org/10.3389/fonc.2015.00272
29. Fernandez-Delgado M, Cernadas E, Barro S, Amorim D (2014) Do we need hundreds of classifiers to solve real world classification problems? J Mach Learn Res 15:3133–3181
30. Hanley JA, Mcneil BJ (1982) The meaning and use of the area under a receiver operating characteristic (ROC) curve. Radiology 143:29–36
31. Delong ER, Delong DM, Clarkepearson DI (1988) Comparing the areas under 2 or more correlated receiver operating characteristic curves - a nonparametric approach. Biometrics 44:837–845
32. Wu J, Sun XL, Wang J et al (2017) Identifying relations between imaging phenotypes and molecular subtypes of breast cancer: model discovery and external validation. J Magn Reson Imaging 46:1017–1027
33. Zweig MH, Campbell G (1993) Receiver-operating characteristic (ROC) plots - a fundamental evaluation tool in clinical medicine. Clin Chem 39:561–577
34. Saeys Y, Inza I, Larranaga P (2007) A review of feature selection techniques in bioinformatics. Bioinformatics 23:2507–2517
35. Coroller TP, Grossmann P, Hou Y et al (2015) CT-based radiomic signature predicts distant metastasis in lung adenocarcinoma. Radiother Oncol 114:345–350
36. Wu W, Parmar C, Grossmann P et al (2016) Exploratory study to identify radiomics classifiers for lung cancer histology. Front Oncol. https://doi.org/10.3389/fonc.2016.00071
37. Huang YQ, Liu ZY, He L et al (2016) Radiomics signature: a potential biomarker for the prediction of disease-free survival in early-stage (I or II) non-small cell lung cancer. Radiology 281:947–957
38. Collewet G, Strzelecki M, Mariette F (2004) Influence of MRI acquisition protocols and image intensity normalization methods on texture classification. Magn Reson Imaging 22:81–91

Affiliations

Xiaochun Meng[1] · Wei Xia[2] · Peiyi Xie[1] · Rui Zhang[2] · Wenru Li[1] · Mengmeng Wang[2] · Fei Xiong[1] · Yangchuan Liu[2] · Xinjuan Fan[3] · Yao Xie[1] · Xiangbo Wan[4] · Kangshun Zhu[5] · Hong Shan[6] · Lei Wang[7] · Xin Gao[2]

[1] Department of Radiology, Sixth Affiliated Hospital of Sun Yat-sen University, Guangzhou 510655, China

[2] Suzhou Institute of Biomedical Engineering and Technology, Chinese Academy of Sciences, 88 Keling Road, Suzhou New District, Suzhou 215163, Jiangsu, China

[3] Department of Pathology, Sixth Affiliated Hospital of Sun Yat-sen University, Guangzhou 510655, China

[4] Department of Radiotherapy, Sixth Affiliated Hospital of Sun Yat-sen University, Guangzhou 510655, China

[5] Department of Interventional Medicine, Second Affiliated Hospital of Guangzhou Medical University, Guangzhou 510260, China

[6] Guangdong Provincial Engineering Research Center of Molecular Imaging, Fifth Affiliated Hospital of Sun Yat-sen University, Zhuhai 519000, China

[7] Department of Colorectal Surgery, Sixth Affiliated Hospital of Sun Yat-sen University, 26 Yuancun Erheng Road, Tianhe District, Guangzhou 519000, Guangdong, China